Stratum corneum model membranes : molecular organization in relation to skin barrier function

Groen, D.

Chapter 4

Investigating the barrier function of skin lipid models with varying compositions

Daniël Groen, Dana S. Poole, Gert S. Gooris, Joke A. Bouwstra

Eur J Pharm Biopharm, in press

Abstract

The lipids in the uppermost layer of the skin, the stratum corneum (SC), play an important role in the barrier function. The main lipid classes in stratum corneum are ceramides, cholesterol and free fatty acids. In previous publications a lipid model was presented, referred to as the stratum corneum substitute (SCS), that closely mimics the SC lipid organization and SC barrier function. In the present study, we use the SCS to study the effect of changes in lipid organization on the lipid barrier function using benzoic acid as permeation compound. First, in the SCS we increased the level of one of the three major lipid classes keeping the ratio between the other lipid classes constant. An increased cholesterol level resulted in an increase in phase separated cholesterol and a reduction in the permeability. An increase in ceramide or free fatty acid level resulted in the formation of additional phases, but had no significant influence on the permeability. We also examined models that mimic selected changes in lipid composition reported for dry or diseased skin. The SCS that mimics the composition in recessive X-linked ichthyosis skin displayed a twofold increase in permeability. This increase is possibly related to the formation of an additional, less ordered phase in this model.

1. Introduction

The physical barrier of the human skin is located in the uppermost layer, the stratum corneum (SC). The SC consists of enucleated dead cells (corneocytes) that are surrounded by lipid lamellae. As these lipid lamellae form a continuous pathway in the SC, the lipid domains are considered to play a dominant role in the skin barrier function (4). The main lipid classes in the SC are ceramides (CER), cholesterol (CHOL) and free fatty acids (FFA) (5-9). The lipids are arranged in two crystalline coexisting lamellar phases with repeat distances of 13 and 6 nm, respectively. These lamellar phases are referred to as the long periodicity phase (LPP) and the short periodicity phase (SPP) (10, 11). At the skin temperature of 30-32ºC, in human SC the lipids in the lipid lamellae are organized mainly in an orthorhombic lateral packing, although a subpopulation of lipids also forms a hexagonal or even a liquid-like lateral packing (12-14). The lateral and lamellar lipid organization are considered to play an important role in the skin barrier function (14-16). When focusing in more detail on the lipid composition, a wide distribution of FFA chain lengths has been identified. The most abundant chain lengths in the FFA mixture are those of 22 and 24 C atoms (17). As far as the CER are concerned, currently, there are eleven subclasses of CER identified in human SC (5, 6, 9). To understand the change in lipid phase behaviour in diseased and dry skin (18-22), we should unravel the complex phase behaviour in SC. As it is impossible to perform these studies with intact SC, lipid mixtures should be used mimicking the lipid phase behaviour of SC as closely as possible. In previous studies lipid mixtures were prepared using isolated as well as synthetic CER mixtures. These lipid mixtures mimicked the lipid organization of SC very closely and provided useful information on the role the lipid classes play in the lipid phase behaviour (23-25). However, no information was obtained about the relation between lipid organization and the skin barrier function. In order to study this, we developed a skin lipid membrane consisting of a porous substrate covered with a mixture of synthetic CER, CHOL and FFA. This membrane is referred to as the stratum

corneum substitute (SCS). The SCS mimics the lipid organization and lipid orientation in SC very closely. As the lipid composition can easily be modified, the SCS allows us to study the relationship between lipid composition, molecular organization and barrier function in just one model (1, 26, 27). In a previous study it was observed that the LPP plays an important role in the skin barrier function (26). In a recent paper we examined also the effect of the lateral packing on the permeability of the SCS using benzoic acid (BA), a medium lipophilic low molecular weight compound, as model drug (2). This study revealed that an orthorhombic to hexagonal transition does not affect the diffusivity of BA in the SCS.

In the present study, we will first systematically change the CER, CHOL and FFA composition. Subsequently we examine models that mimic some aspects of the changes in lipid composition reported for SC of dry skin (winter xerosis), recessive X-linked ichthyosis and psoriasis skin. The permeability of the in vitro SCS models is assessed by measuring the permeation of BA. To examine the lipid organization in the models, Fourier transform infrared spectrometry (FTIR) and small-angle X-ray diffraction (SAXD) are used.

2. Materials and Methods

2.1 Materials

Synthetic CER(EOS)C30-linoleate, CER(EOS)C30-oleate, CER(NS)C24, CER(NP)C24, CER(NP)C16, CER(AS)C24 and CER(AP)C24 (see figure 1) were generously provided by Cosmoferm B.V. (Delft, The Netherlands). Palmitic acid (C16:0), stearic acid (C18:0), arachidic acid (C20:0), behenic acid (C22:0), tricosanoic acid (C23:0), lignoceric acid (C24:0), cerotic acid (C26:0) and cholesterol were purchased from Sigma-Aldrich Chemie GmbH (Schnelldorf, Germany). Benzoic acid was obtained from Sigma-Aldrich (Zwijndrecht, The Netherlands). Nuclepore polycarbonate filter disks (pore size 50 nm) were purchased from Whatman

(Kent, UK). All organic solvents are of analytical grade and manufactured by Labscan Ltd. (Dublin, Ireland). All other chemicals are of analytical grade and the water is of Millipore quality.

Table 1:

model type	abbreviation	composition and molar ratio	J_{ss} (µg/cm^2/h)	τ (h)
SC substitute	SCS	CER : CHOL : FFA 1 : 1 : 1	24 ± 2 †	1.1 ± 0.5 †
high CER level		CER : CHOL : FFA 2 : 1 : 1	22.5 ± 1.8	-0.3 ± 0.5
high CHOL level		CER : CHOL : FFA 1 : 2 : 1	9.0 ± 1.5	0.6 ± 0.6
high FFA level		CER : CHOL : FFA 1 : 1 : 2	25.6 ± 1.2 #	n.a.
psoriasis model	PS SCS	CER : CHOL : FFA 1 : 1.2 : 0.5	14.5 ± 1.1	0.3 ± 0.2
winter xerosis model	WX SCS	CER*: CHOL : FFA 1 : 1 : 1	15.6 ± 2.6	0.9 ± 0.8
recessive X-linked ichtyosis	RXLI SCS	CER : CHOL : FFA : $ChSO_4$ 1 : 1 : 1 : 0.33	46.2 ± 5.5	0.1 ± 0.3

*** In the CER composition of the winter xerosis model 50% of the CER(EOS)-linoleate is replaced by CER(EOS)-oleate.**

† For the equimolar SCS, J_{ss} and τ were obtained in a previous study (1).

 # For the SCS with a high FFA level, J_{ss} was determined from the last 4 flux values, therefore τ could not be calculated.

2.2 Preparation of the model lipid mixtures

For the preparation of the SCS models, CHOL, synthetic CER and FFA were used in the appropriate molar ratio according to the different models. In Table 1 the ratios of the main lipid classes are displayed for the models used in this study. The main CER subclasses we have available consist of either a sphingosine (S) or phytosphingosine (P) base, whereas the acyl chain is a nonhydroxy (N), α-hydroxy (A) or ω-hydroxy chain (3). The corresponding nonhydroxy and α-hydroxy CER that are used in this study are denoted as CER NP, CER NS, CER AP and CER AS. The ω-hydroxy CER possesses a longer acyl chain length (C30) and has a linoleic or oleic acid ester-linked to their ω-hydroxy group (indicated with EO). In our study we use two such acylCERs, denoted as CER(EOS)-linoleate and CER(EOS)-oleate. For the ceramides mixture (CER) the following synthCER

composition was selected (see figure 1): CER(EOS)C30-linoleate, CER(NS)C24, CER(NP)C24, CER(AS)C24, CER(NP)C16 and CER(AP)C24 in a 15:51:16:4:9:5 molar ratio, similar as observed in pig SC (25). The acyl chain length of the various CER subclasses is either 30 C atoms (C30), 24 C atoms (C24) or 16 C atoms (C16). For the free fatty acids mixture (FFA), the following composition was selected: C16:0, C18:0, C20:0, C22:0, C23:0, C24:0 and C26:0 at a molar ratio of 1.8:4.0:7.7:42.6:5.2:34.7:4.1 respectively. This chain length distribution is based on the reported FFA composition in SC (17). For each model the appropriate amounts of individual lipids were dissolved in chloroform:methanol (2:1 v/v). After evaporation of the organic solvent under a stream of nitrogen, the lipid mixtures were re-dissolved either in hexane:ethanol 2:1 v/v (for models used in permeability and X-ray studies) or in chloroform:methanol 2:1 v/v (for models used in FTIR studies) at a total lipid concentration of 4.5 mg/ml.

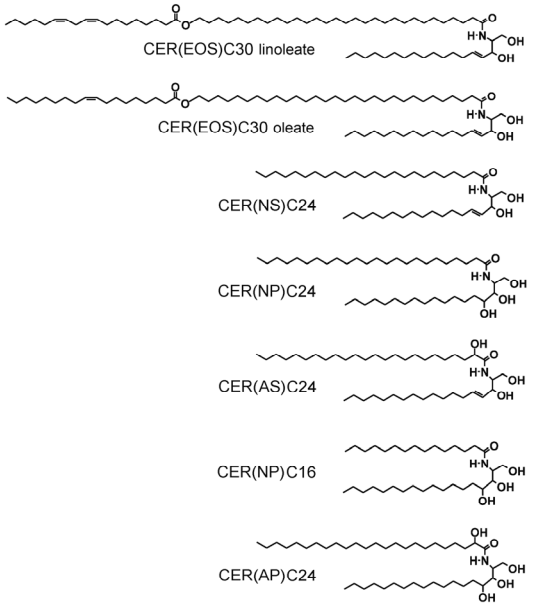

Figure 1: Molecular structure of the synthetic CER selected for the lipid mixtures (see Table 1). The nomenclature is according to Motta et al (3).

2.3 Preparation of SCS models for in vitro permeability studies

A Linomat IV (Camag, Muttenz, Switzerland) extended with a y-axis arm was used to spray lipids in hexane:ethanol solution from a distance of 1 mm onto a porous filter substrate. The spraying flow rate was 5.0 µl/min at a movement speed of 1.0 cm/s. In an area of 8×8 mm^2 0.90 mg of lipids was applied per SCS model. After spraying, the SCS was equilibrated at around 80ºC. After an equilibration period of at least 10 minutes, the SCS was cooled down to room temperature in approximately 30 minutes.

2.4 Preparation of lipid models for FTIR studies

Sample preparation for FTIR was the same as above, but instead 1.5 mg of lipids in a chloroform:methanol solution was sprayed in an area of 1x1 cm^2 on an AgBr window. The sample was equilibrated for 10 min at around 80ºC and slowly cooled down to room temperature in about 30 min. Subsequently, the lipid layer was covered with 25 µl of deuterated acetate buffer pH 5 (50 mM) and stored at 37°C for 24h to fully hydrate the sample. Finally, to homogenize the sample, five freeze-thawing cycles of 3h each were carried out between -20°C and RT (28).

2.5 Permeability studies

In vitro permeation studies were performed using Permegear inline diffusion cells (Bethlehem PA, USA) with a diffusion area of 0.28 cm^2. The SCS models were mounted in the diffusion cells and were hydrated for 1 h in phosphate-buffered saline (PBS: NaCl, Na_2HPO_4, KH_2PO_4 and KCL in MQ water with a concentration of 8.13, 1.14, 0.20 and 0.19 g/l respectively) at pH 7.4 prior to the experiment. The donor compartment was filled with 1.4 ml of BA (MW 122 g/mol) solution in PBS (pH 7.4) at a 2.0 mg/ml concentration. BA has a log $P_{oct/water}$ value of about 1.7. The acceptor phase consisted of PBS (pH 7.4), which was perfused at a flow rate of about 2 ml/h. The acceptor phase was stirred with a magnetic stirrer. The volume per collected fraction was determined by weighing. Each experiment was performed under

occlusive conditions, by closing the opening of the donor compartment with adhesive tape. To mimic the in vivo conditions as close as possible the temperature of the SCS was maintained at 32°C during the permeation studies, using a thermo-stated water bath.

Steady state fluxes and lag-times were determined from a plot of the cumulative permeated amount. The steady state flux (J_{SS}) is the slope of the linear part of this graph and the lag-time (τ) is determined by regression of this linear part to the time when the permeated amount is 0.

2.6 FTIR studies

All spectra were acquired on a BIORAD FTS4000 FTIR spectrometer (Cambridge, Massachusetts) equipped with a broad-band mercury cadmium telluride detector, cooled with liquid nitrogen. The sample cell was closed by two AgBr windows. The sample was under continuous dry air purge starting 1 hour before the data acquisition. The spectra were collected in transmission mode, as a co-addition of 256 scans at 1 cm^{-1} resolution during 4 minutes. In order to detect the phase transitions, the sample temperature was increased at a heating rate of 0.25˚C/min, resulting in a 1°C temperature rise per recorded spectrum. The spectra were collected between 0˚C and 90˚C. The software used was Win-IR pro 3.0 from Biorad (Cambridge, Massachusetts). The spectra were deconvoluted using a half-width of 5 cm^{-1} and an enhancement factor of 2.0.

2.7 Determining the midpoint temperature of the melting transition and fitting of the rocking vibrations in FTIR

In FTIR, the frequency of the symmetric stretching maximum as function of temperature depicts the transition of the lipids to a liquid phase (29, 30). The midpoint temperature (T_m) of the melting transition was determined as the temperature at which the frequency increase is halfway between two fitted straight parts of the curve before and after the transition. The straight parts before and after the transition are fitted by linear fits and

the data point closest to the transition that deviates from the linear fit is chosen as the beginning or end point of the melting transition. This method for determining T_m is depicted in figure 2B-ii.

The frequency of the two rocking maxima as function of temperature depict the phase transition from an orthorhombic to a hexagonal lateral packing (31, 32). During this transition, at those temperatures at which no separate peaks could be distinguished but only an asymmetric peak, two components were fitted to the rocking vibrations in order to determine the position of the high-frequency component. The curve-fitting procedure was as follows: First, in the range from 635 to 900 cm^{-1} in the FTIR spectrum a baseline was created with a constant value corresponding to the lowest value in that part of the spectrum. Subsequently the two components present in the spectrum were fitted with two Lorentzian peak shapes using a least squares approximation. The position of the maximum of the high-frequency component was subsequently used in the plot of the rocking frequencies as function of temperature. In this plot, the positions of the high-frequency component are displayed until a temperature is reached at which the high-frequency component could no longer be fitted.

2.8 SAXD studies

X-ray diffraction was used to obtain information about the lamellar organization (i.e., the repeat distance of a lamellar phase) and the orientation of the lamellae. The SCS was mounted parallel to the primary beam in a temperature controlled sample holder with mica windows. Static diffraction patterns were collected for 1 minute at 25°C. The scattering intensity I (in arbitrary units) was measured as a function of the scattering vector q (in reciprocal nm). The latter is defined as $q=(4\pi\sin\theta)/\lambda$, in which θ is the scattering angle and λ is the wavelength. From the positions of a series of equidistant peaks (q_n), the periodicity, or d-spacing, of a lamellar phase was calculated using the equation $q_n=2n\pi/d$, with n being the order number of the diffraction peak. One-dimensional intensity profiles were

obtained by transformation of the two-dimensional SAXD detector pattern from Cartesian (x,y) to polar (ρ,θ) coordinates and subsequently integrating over θ. All measurements were performed at the European Synchrotron Radiation Facility (ESRF, Grenoble) using station BM26B. The X-ray wavelength and the sample-to-detector distance were 0.113 nm and 0.419 m respectively. Diffraction data were collected on a Frelon 2000 CCD detector with 2048×2048 pixels at 14 μm spatial resolution and 5x magnification. The spatial calibration of this detector was performed using silver behenate (d=5.838 nm) and the two strongest reflections of high density polyethylene (HDPE, d=0.4166 and 0.378 nm).

3. Results

To assess the barrier properties of the various SCS models, the permeation of the model compound BA has been measured at the skin temperature of about 32°C. To correlate permeability with lipid organization, the lipid organization has been examined with FTIR and SAXD. The various model compositions, steady state flux values and lag-times are presented in Table 1.

3.1 Influence of the CER:CHOL:FFA ratio on the barrier function

To determine the role of each of the lipid classes on the lipid composition and permeability, SCS varying systematically in CER:CHOL:FFA composition were examined. The fluxes are provided in Table 1. In this table the flux across SCS with an equimolar CER:CHOL:FFA composition that was reported previously (1), is also provided. In figure 2A-i the BA flux profile across the SCS with a CER:CHOL:FFA molar ratio of 2:1:1 is shown. The steady state flux is 22.5 ± 1.8 μg/cm^2/h and the lag-time is -0.3 ± 0.5 h.

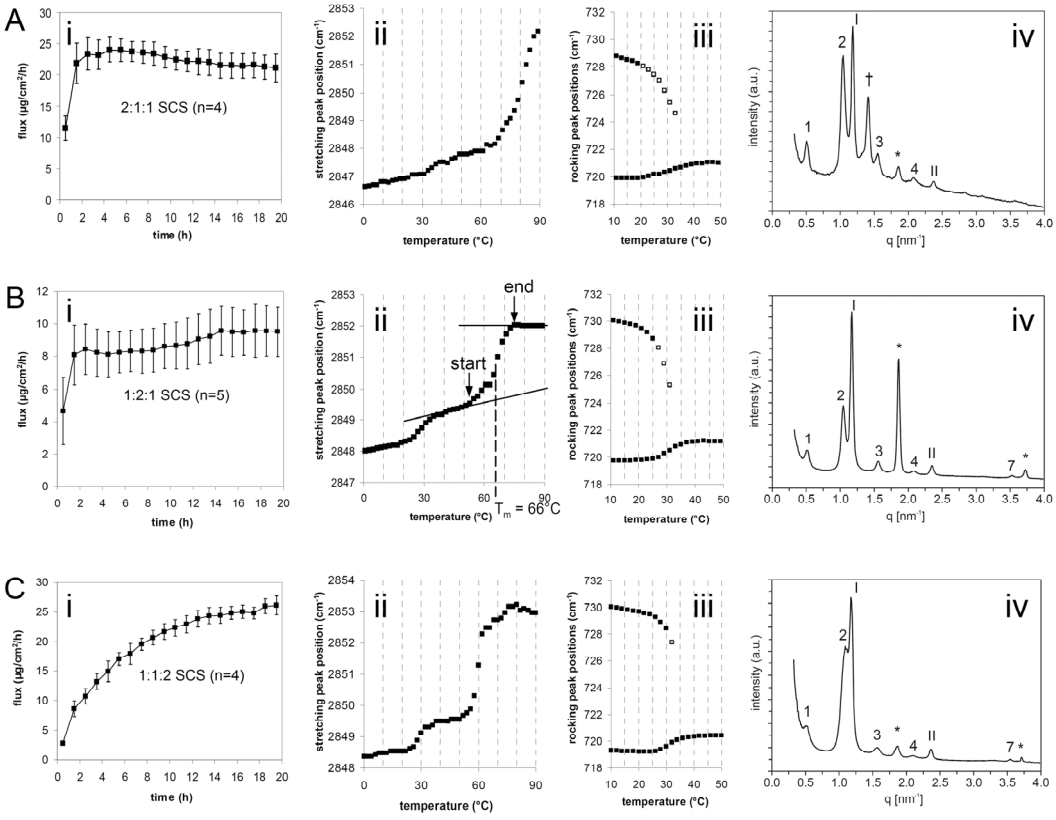

Figure 2: i) Plots of the BA permeation versus time, ii) CH_2 symmetric stretching frequency as function of temperature, iii) thermotropic response of the FTIR CH_2 rocking frequencies and iv) the SAXD pattern of A) SCS in 2:1:1 CER:CHOL:FFA molar ratio, B) SCS in a 1:2:1 CER:CHOL:FFA molar ratio C) SCS in a 1:2:1 CER:CHOL:FFA molar ratio. In the SAXD patterns, the Arabic numbers denote diffraction orders of the LPP, the Roman numbers indicate reflections assigned to the SPP and asterisks mark the reflections of crystalline CHOL. The reflection that was assigned to an additional lamellar phase is indicated by a cross. In the figures depicting the CH_2 rocking vibrations the open squares are calculated with the peak fitting procedure.

The CH_2 symmetric stretching frequencies in the infrared spectrum provide information about the conformational ordering of the lipid tails. The

position of the CH_2 symmetric stretching vibration as function of temperature is plotted in figure 2A-ii. At 20°C this frequency is 2846.9 cm^{-1}, indicating a high conformational ordering. When increasing the temperature, between 30 and 40°C a weak shift is observed in frequency from 2847.1 to 2847.5 cm^{-1}. Although not very pronounced, it indicates an orthorhombic to hexagonal transition. Increasing the temperature leads to another shift in frequency from 2848.1 to 2852.2 cm^{-1} between 65 and 89°C, revealing the transition to a liquid phase, with a midpoint temperature of T_m = 80°C.

The FTIR rocking frequencies provide detailed information on the lateral packing. Due to short range coupling, the orthorhombic packing is characterized by a doublet at approximately 720 and 730 cm^{-1}, while the hexagonal packing is characterized by a singlet at a vibration frequency of approximately 720 cm^{-1}. The thermotropic response of the rocking frequencies in figure 2A-iii shows a shift of the high frequency component from 728.0 to 724.6 cm^{-1} between 21 and 33°C, suggesting the transition from an orthorhombic to a hexagonal lateral packing in this temperature region.

The SAXD pattern of the 2:1:1 SCS in figure 2A-iv displays four diffraction peaks that can be ascribed to a LPP with a periodicity of 12.0 nm and two reflections attributed to a SPP with periodicity of 5.3 nm. Furthermore, an additional diffraction peak is observed indicative for an additional phase with a periodicity of 4.4 nm, most likely due to phase separated CER-rich domains. The peak at q = 1.85 nm^{-1} indicates the presence of a low level of phase separated crystalline CHOL.

The SCS with elevated CHOL level was also studied. The permeability of the SCS with a CER:CHOL:FFA composition of 1:2:1 is displayed in figure 2B-i. This figure demonstrates that by increasing the CHOL levels the BA flux drastically reduces since the steady state flux is only 9.0 ± 1.5 $\mu g/cm^2/h$. The lag-time of this membrane is 0.6 ± 0.6 h.

The thermotropic response of the CH_2 stretching frequencies is provided in figure 2B-ii. There is a gradual increase in the frequencies from 0

to 20°C. At 20°C, the symmetric stretching frequency is 2848.3 cm^{-1}, denoting the presence of conformational ordered phases. A further increase in temperature from 21 to 37°C results in a shift in frequency from 2848.3 to 2849.1 cm^{-1}, indicative for the orthorhombic-hexagonal phase transition. Upon further heating, between 50 and 79°C a second transition is observed from 2849.4 to 2852.0 cm^{-1}, demonstrating the formation of a liquid phase. The midpoint temperature of this transition is 66°C.

The rocking frequencies are displayed in figure 2B-iii. The orthorhombic to hexagonal transition is shown by a shift of the high frequency component from 729.5 to 725.3 cm^{-1} between 21 and 31°C.

The SAXD pattern of the 1:2:1 SCS is displayed in figure 2B-iv with diffraction peaks attributed to the LPP and SPP. However, the diffraction peaks attributed to crystalline CHOL have a high intensity, demonstrating a high level of phase separated CHOL.

The level of the third main class of lipids is also increased in the SCS. In figure 2C-i the permeability curve of SCS with a CER:CHOL:FFA molar ratio of 1:1:2 is displayed. From this figure it is clear that a steady state flux is not reached within the 20 h of permeation. The flux value was calculated as a mean of the flux values between 16 and 20 h of permeation and is 25.6 ± 1.2 $\mu g/cm^2/h$. The lag-time could not be determined due to the absence of a steady state flux.

The thermotropic CH_2 stretching response is provided in figure 2C-ii. At low temperatures the lipid tails are in a conformational ordering as shown by the CH_2 stretching frequency of 2848.6 cm^{-1} at 20°C. Upon increasing the temperature, a clear shift in frequency from 2848.6 to 2849.5 cm^{-1} is observed between 22 and 38°C, demonstrating the orthorhombic to hexagonal phase transition. When further increasing the temperature, another shift in wavenumber from 2849.6 to 2852.8 cm^{-1} is visible between 50 and 72°C denoting the transition to a liquid phase with a midpoint temperature of 60°C.

The orthorhombic to hexagonal phase transition is also monitored by the thermotropic CH_2 rocking response as displayed in figure 2C-iii: A shift of the high frequency component from 729.5 to 727.4 cm^{-1} is observed between 24 and 32°C. When increasing the temperature further a weak orthorhombic component remained in the rocking curve until a temperature of 60°C. This indicates that the majority of the lipids forms a hexagonal lateral packing around 34°C, but a small fraction of phase separated FFA remains in the orthorhombic packing until a temperature of about 60°C is reached (28). At this temperature the crystalline FFA starts to transform into a liquid phase.

The SAXD pattern of the model with high FFA level is displayed in figure 2C-iv. It depicts two diffraction peaks attributed to the SPP with a periodicity of 5.3 nm. Five diffraction peaks could be identified that are attributed to the LPP with a periodicity of 12.0 nm. The two peaks at q = 1.85 and 3.7 nm^{-1} indicate the presence of a low level of phase separated crystalline CHOL. The elevated FFA level did not result in an additional phase with a long range ordering.

3.2 The permeability and phase behaviour of SCS with a lipid composition based on that in dry or diseased skin

The lipid organization and barrier properties of models with compositions related to dry skin (winter xerosis), recessive X-linked ichthyosis and psoriasis skin were also examined.

Due to seasonal influences the lipid composition in the SC is reported to undergo changes. Focussing on the CER subclasses, in the winter season the relative level of CER(EOS)-oleate is increased at the expense of CER(EOS)-linoleate (21, 33). To mimic this aspect of the SC composition of dry skin (winter xerosis), 50% of the CER(EOS)-linoleate was replaced by CER(EOS)-oleate in the SCS. The SCS that mimics the composition in SC of dry skin is referred to as WX SCS. The permeation

curve of BA through WX SCS is displayed in figure 3A-i. The steady state flux is 15.6 ± 2.6 µg/cm^2/h and the lag-time 0.9 ± 0.8 h.

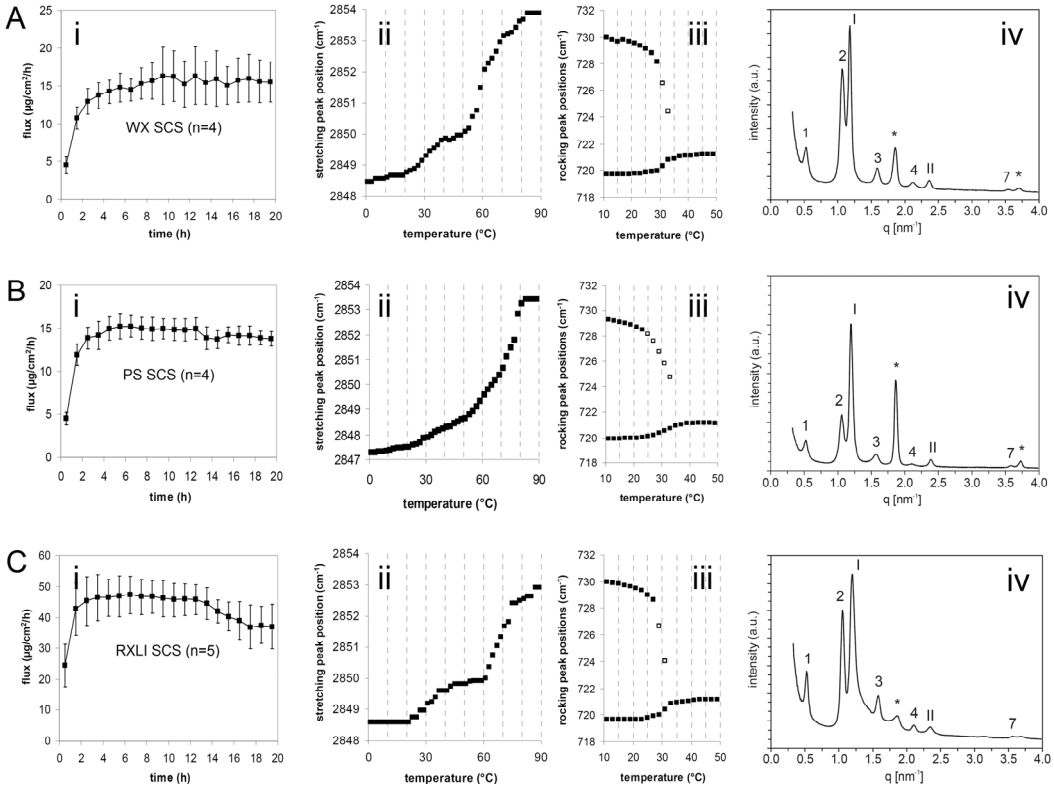

Figure 3: i) Plots of the BA permeation versus time, ii) CH_2 symmetric stretching frequency as function of temperature, iii) thermotropic response of the FTIR CH_2 rocking frequencies and iv) the SAXD pattern of A) WX SCS, B) PS SCS and C) RXLI SCS. In the SAXD patterns, the Arabic numbers denote diffraction orders of the LPP, the Roman numbers indicate reflections assigned to the SPP and asterisks mark the reflections of crystalline CHOL. In the figures depicting the CH_2 rocking vibrations the open squares are calculated with the peak fitting procedure.

The thermotropic response of the CH_2 symmetric stretching peak is plotted in figure 3A-ii. At low temperatures, a gradual increase in frequency is observed up to 2848.7 cm^{-1} at 20°C. Upon increasing the temperature from 21 to 41°C a shift in wavenumber from 2848.8 to 2849.9 cm^{-1} is detected, indicating the orthorhombic to hexagonal phase transition. When further increasing the temperature, a liquid phase is formed between 51 and 73°C as denoted by a shift from 2850.1 to 2853.2 cm^{-1}. The midpoint temperature of this transition is 60°C.

The FTIR rocking frequencies displayed in figure 3A-iii show a shift of the high frequency component from 729.1 to 724.4 cm^{-1} between 25 and 33°C, characteristic for the orthorhombic-hexagonal transition.

The SAXD pattern of WX SCS is shown in figure 3A-iv. It displays two diffraction peaks attributed to a SPP with a periodicity of 5.3 nm and five diffraction peaks assigned to the LPP with a periodicity of 12.0 nm. Crystalline CHOL is also present, as indicated by two diffraction peaks at q = 1.85 and 3.7 nm^{-1}.

Besides a change in CER:CHOL:FFA molar ratio, a difference in the CER composition of psoriatic scale, compared to normal human stratum corneum, is reported in literature (3, 20). However, in our present studies we will only focus on the change in CER:CHOL:FFA molar ratio on the permeability, to establish whether this change can account for an increased permeability in psoriasis skin. Based on the results of Motta et al, the CER:CHOL:FFA molar ratio in the SCS model was adapted to 1.0:1.2:0.5 (20). This model is referred to as PS SCS. The flux profile of PS SCS is displayed in figure 3B-i, displaying a steady state flux of 14.5 ± 1.1 $\mu g/cm^2/h$ and a lag-time of 0.3 ± 0.2 h.

The thermotropic response of the CH_2 stretching vibrations is displayed in figure 3B-ii. The maximum of the symmetric stretching frequencies at 20°C is 2847.5 cm^{-1}. Upon increasing the temperature, a small shift in peak position is visible around 30°C, possibly revealing the orthorhombic to hexagonal transition. Upon further heating, a shift in

wavenumber is visible between 50 and 80°C, indicative for the transition to a liquid phase. This transition has a T_m of 72°C.

The FTIR rocking frequencies in figure 3B-iii show a gradual shift of the high frequency component from 728.2 to 724.8 cm^{-1} between 25 and 33°C, indicating the transition from orthorhombic to hexagonal lateral packing.

The SAXD pattern of PS SCS is depicted in figure 3B-iv. It displays two diffraction orders associated to a SPP, with a periodicity of 5.2 nm. Also, four diffraction peaks assigned to a LPP with a periodicity of 12.0 nm are observed. A high amount of CHOL is phase separated as reflected by the high intensity of the diffraction peaks attributed to crystalline CHOL.

The pathological scaling in recessive X-linked ichthyosis skin is associated with accumulation of abnormally high quantities of $ChSO_4$ in the SC (18, 19, 22). On this basis, we prepared a model for the lipid composition by addition of $ChSO_4$ at a molar ratio of 0.33. This model is referred to as RXLI SCS. The permeation curve of BA through RXLI SCS is displayed in figure 3C-i, showing a high steady state flux of 46.2 ± 5.5 $\mu g/cm^2/h$ and a short lag-time of 0.1 ± 0.3 h.

The FTIR stretching maxima in figure 3C-ii display a constant value of 2848.6 cm^{-1} from 0 to 20°C, indicating conformational ordering of the lipid tails. Upon increasing the temperature, a first shift from 2848.6 to 2849.6 cm^{-1} is observed between 20 and 40°C, representative for an orthorhombic to hexagonal transition. Further increasing the temperature leads to a second shift in wavenumber from 2849.9 to 2852.4 cm^{-1} between 59 and 77°C, representing the transition to a fluid phase with a midpoint temperature of 68°C.

The FTIR rocking frequencies of RXLI SCS in figure 3C-iii reveal a change from orthorhombic to hexagonal transition as shown by a change in high frequency component from 729.0 to 724.0 cm^{-1} between 25 and 31°C.

The SAXD pattern of RXLI SCS is displayed in figure 3C-iv. It displays two diffraction peaks attributed to a SPP with a periodicity of 5.3

nm. The first order reflection of the SPP is broad and contains a shoulder at approximately q = 1.4 nm^{-1} which could indicate the formation of an additional phase. Furthermore, five diffraction peaks are observed assigned to the LPP with a periodicity of 12.0 nm. The two diffraction peaks that are associated to crystalline CHOL are low in intensity, indicating a low level of phase separated CHOL.

4. Discussion

In the studies described in this paper we focused on a systematic change in lipid composition to relate lipid composition and organization with permeability. For this purpose we utilized a SC model membrane to unravel the role the various lipid classes play in the skin barrier function. In addition we focused on the lipid permeability in diseased and dry skin. For this purpose we constructed models for the SC lipid composition reported in winter xerosis, psoriasis and recessive X-linked ichtyosis skin. To study the permeability of the various models we used BA as a model drug.

4.1 The order-disorder transition temperature is related to the symmetric CH_2 stretching vibrations of the lipid tails at 20°C

When closely examining the FTIR data of all models it is observed that the models with a high conformational order at room temperature (i.e. low wavenumber of the CH_2 symmetric stretching peak position at 20°C) exhibit a relatively high melting transition midpoint temperature. To gain more insight into this relationship we plotted the CH_2 symmetric stretching vibration at 20°C against the midpoint temperature of the melting transition in each model, see figure 4. Although the midpoint temperature of the melting transition has no physical meaning, as the symmetric stretching peak in FTIR is composed of several vibrational components, it enables us to determine whether this phase transition is related to the conformational order of the lipid chains at 20°C. We also included data of the equimolar SCS and

a model with short chain FFA, examined in a previous study (2). As depicted in figure 4, a linear correlation is observed: the symmetric stretching wavenumber (chain conformation) at 20°C decreases linearly with increasing melting transition T_m.

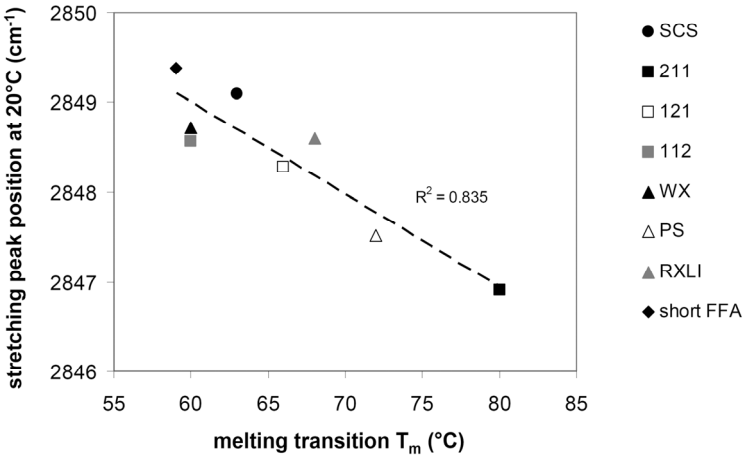

Figure 4: The midpoint temperature of the melting transition as function of the conformational order at 20°C. Depicted are data of all models used in this study plus data of equimolar SCS and of a model with short chain FFA, examined in a previous study (2).

From this graph it is clear that when using the same ceramide composition, an increase in conformational ordering results in an increase in the melting transition T_m. When focusing on those samples in which the FFA content varied, the results are quite remarkable. Although the FFA induces the formation of an orthorhombic lateral packing, it also induces a reduction in the ordering of the chains and a reduction in the T_m. This might be due to the change in headgroup interactions, as it has been suggested (based on pure ceramides but also on mixtures) that an increase in hydrogen bond density in the headgroup region increases the conformational ordering and raises the T_m of the order-disorder transition (34, 35). This suggests that the

addition of FFA increases the packing density but reduces the number of hydrogen bonds.

4.2 Deviation from the equimolar CER:CHOL:FFA ratio observed in human SC does not always result in a decreased barrier function

As it has been suggested that the lipid composition and organization play an important role in the skin barrier, in this study we examined the effect of the lipid composition and organization of the SCS on its permeability. In previous studies we reported the permeability and lipid phase behavior of the equimolar CER:CHOL:FFA SCS, mimicking the lipid composition and skin barrier of healthy subjects (1, 2). The BA steady state flux across this SCS was 24 ± 2 μg/cm^2/h and the lag-time was 1.1 ± 0.5 h (1). From the FTIR data presented in a recent study (2), the midpoint temperature of the transition from a hexagonal to a liquid phase was 63°C and the orthorhombic-hexagonal transition occured between 20 and 36°C. In the same study we observed that the flux of BA was more sensitive for a change in the lamellar phases than for a phase change from an orthorhombic to a hexagonal packing. In the present study we varied the lipid composition by increasing the level of either CER, CHOL or FFA. The formation of a hexagonal phase in these studies is not determinative for the changes in flux.

When increasing the level of CER or CHOL by a factor two compared to the equimolar ratio, the X-ray diffraction curves clearly revealed phase separation. In the SCS with 2:1:1 CER:CHOL:FFA an additional 4.4 nm phase was detected, while the CER:CHOL:FFA 1:2:1 SCS resulted in an enhanced level of phase separated crystalline CHOL. The additional 4.4 nm phase did not affect the permeability, while the higher level of phase separated CHOL in the SCS led to a twofold reduction in the permeability. The CHOL domains consist of densely packed three dimensional crystals resulting in many spots and reflections in the WAXD pattern (not shown). If

these three dimensional crystals are not very permeable to BA, it will result in a reduction of the effective diffusion area of the SCS and in an increase in the permeation pathway. This will lead to a reduction in the steady state flux. As far as the 4.4 nm phase is concerned, our results indicate that this phase has a similar layered structure as the SPP as no features in the diffraction pattern are observed indicating the presence of a three dimensional crystalline structure (wide angle X-ray data, unpublished results). This may explain why no change in permeability is observed in the presence of the 4.4 nm phase.

When comparing with the in vivo situation, the 4.4 nm phase was never observed in diffraction patterns of isolated human SC. However, the presence of crystalline CHOL is frequently observed in human SC (11, 36). Therefore, the observation that an increase in phase separated crystalline CHOL results in an increase in the skin barrier function is relevant for the in vivo situation.

In the 1:1:2 CER:CHOL:FFA SCS no phase separation of FFA is observed when focusing on the long range ordering (lamellar phases). However, the presence of a small shoulder was noticed in the high frequency component of the FTIR rocking vibrations. This shoulder was present up to about 60°C and indicates that a low level of FFA forms separate domains within the lipid lamellae. The flux of BA across the 1:1:2 CER:CHOL:FFA SCS displays a very long lag-time. As we used a PBS buffer of pH 7.4 in the donor and acceptor phase and the pK_a of FFA in ceramide containing mixtures is around 6.3 (37), the increase in lag-time may occur by an ionization of the FFA, which may be more pronounced at a high level of FFA, or in phase separated FFA domains within the lipid lamellae.

As far as the diseased skin models are concerned, in these studies we are limited by the information available in literature. Although changes in the composition of the lipid classes have been reported for cosmetically dry skin and for psoriasis, no information is available on the FFA and CER chain

length distribution compared to that in skin of healthy subjects. A reduction in chain length of the CER and FFA may have a profound effect on the lipid organization and permeability. For this reason our studies only provide information on the changes in permeability caused by the reported changes in the composition of the main lipid classes in the various skin diseases.

For both the WX SCS and PS SCS the steady state flux and lag-time is similar to that in the equimolar CER:CHOL:FFA SCS. The lamellar lipid organization of these models is also similar to that in the equimolar SCS and as the lamellar organization is a crucial factor in the skin permeability (2, 14), it is not surprising that the WX SCS and PS SCS have a barrier function that is similar to the equimolar SCS. Although winter xerosis skin is known to be susceptible and displays a faulty desquamation (38, 39) and psoriasis skin is characterized by a deranged keratinization process and an impaired barrier function (40), our results with BA as permeant demonstrate that the reported changes in CER(EOS)-oleate/linoleate ratio in dry skin or in CER:CHOL:FFA ratio in psoriasis skin may not be responsible for the observed impaired barrier function in vivo.

In contrast to the WX and PS models, the permeability of the RXLI model is about twice that of equimolar SCS. Therefore the enhanced permeability indicates that the increased $ChSO_4$ is expected to be at least partly responsible for the abnormal barrier function observed in RXLI skin (22). The reduced barrier function in our lipid model may partly be explained by the lower level of phase separated crystalline CHOL: The excess $ChSO_4$ present in this model reduces the amount of crystalline CHOL, similarly as previously observed in a lipid model with isolated CER (41). However, the reduced crystalline CHOL cannot explain the twofold increase in flux as the level of phase separated crystalline CHOL in the 2:1:1 and 1:1:2 CER:CHOL:FFA SCS was also lower, while no increase in permeability was observed. Therefore, other factors should play a role. Previously it was observed that $ChSO_4$ induces a fluid phase in mixtures with isolated CER, CHOL and FFA (42). Such a fluid phase is expected to increase the

permeability. However, at room temperature (20°C) the frequency of CH_2 symmetric stretching vibrations of the RXLI model was not shifted to a higher wavenumber as compared to equimolar SCS, indicating that the formation of a substantial level of fluid phase in SCS was not induced by the addition of $ChSO_4$. Perhaps the use of synthetic CER instead of isolated CER precludes the formation of a fluid phase in the RXLI SCS. In order to explain the increased permeability, we investigated the two dimensional SAXD patterns in more detail and examined the equimolar and RXLI SCS also under a polarization microscope. When examining the two dimensional detector image of the RXLI model, we observed that the increased level of $ChSO_4$ induces a well oriented but broad reflection, close to the position of the first order of the SPP, see figure 5. Also higher order broad reflections of this phase are observed. This indicates that an additional phase is present in the SCS. The less sharp reflections suggest a less ordered phase, which may account for the increased permeability.

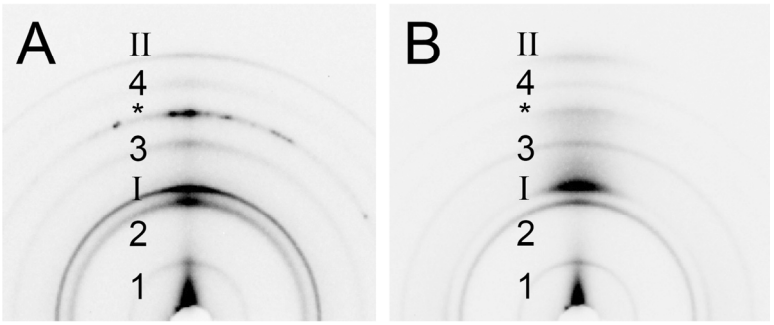

Figure 5: Two dimensional SAXD images. The Arabic numbers 1-4 denote diffraction orders of the LPP, the reflections indicated by Roman numbers I and II are assigned to the SPP and a reflection of crystalline CHOL is indicated with an asterisk. A) Diffraction pattern of the equimolar SCS B) Diffraction pattern of the RXLI model. Broader reflections are located in the centre of the ring at the same position as the 1st and 2nd order of the SPP, indicating an oriented but more disordered additional phase. The intensity of the CHOL reflection is also strongly reduced.

When further examining the RXLI model under a polarization microscope, we observed large patches that are absent in the equimolar SCS, see figure 6, confirming that an additional phase is formed by supplementing $ChSO_4$.

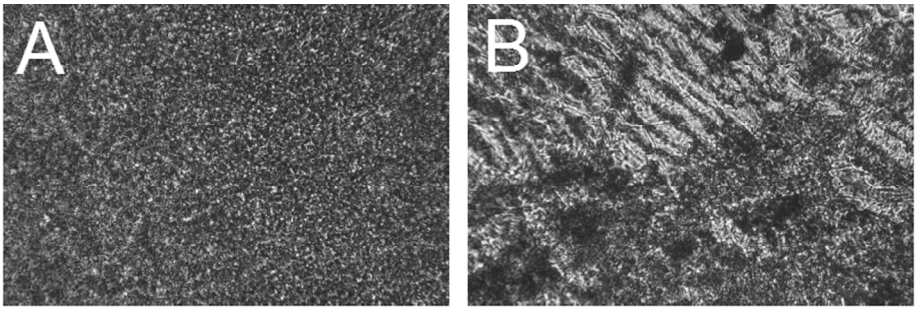

Figure 6: Polarization microscopy images using a 40x magnification. A) Equimolar SCS, displaying a uniform pattern of small domains B) The RXLI SCS, displaying large irregularly shaped domains.

In conclusion, in our studies two SCS models showed a significant change in BA steady state flux; an excess of crystalline CHOL lead to a decreased steady state flux, while an excess of $ChSO_4$, as observed in X-linked ichthyosis, led to an increase in the BA steady state flux. While phase separated CHOL is crystalline and therefore possibly difficult to penetrate, there is some evidence that the additional phase induced by $ChSO_4$ is less ordered in nature accounting for the increased permeability. A change in CER:CHOL:FFA ratio in psoriasis skin and an increase in the CER EOS-oleate/CER EOS-linoleate ratio in dry skin may not be responsible for the impaired skin barrier function in vivo.

Acknowledgments

This work was supported by a grant from the Technology Foundation STW (LGP 7503). We thank the company Cosmoferm B.V. (Evonik) for the provision of the ceramides and the Netherlands Organization for Scientific Research (NWO) for the provision of beam time at the ESRF. Furthermore, we thank the personnel at the DUBBLE beam line at the ESRF for their support with the X-ray measurements. Finally, we thank Dr Maria Ponec for valuable discussions on the permeability studies.

References

1. Groen, D., G. S. Gooris, M. Ponec, and J. A. Bouwstra. 2008. Two new methods for preparing a unique stratum corneum substitute. Biochim Biophys Acta 1778:2421-2429.
2. Groen, D., D. S. Poole, G. S. Gooris, and J. A. Bouwstra. 2010. Is an orthorhombic lateral packing and a proper lamellar organization important for the skin barrier function? Biochim Biophys Acta.
3. Motta, S., M. Monti, S. Sesana, R. Caputo, S. Carelli, and R. Ghidoni. 1993. Ceramide composition of the psoriatic scale. Biochim. Biophys. Acta 1182:147-151.
4. Simonetti, O., A. J. Hoogstraate, W. Bialik, J. A. Kempenaar, A. H. Schrijvers, H. E. Bodde, and M. Ponec. 1995. Visualization of diffusion pathways across the stratum corneum of native and in-vitro-reconstructed epidermis by confocal laser scanning microscopy. Arch Dermatol Res 287:465-473.
5. Masukawa, Y., H. Narita, E. Shimizu, N. Kondo, Y. Sugai, T. Oba, R. Homma, J. Ishikawa, Y. Takagi, T. Kitahara, Y. Takema, and K. Kita. 2008. Characterization of overall ceramide species in human stratum corneum. J Lipid Res 49:1466-1476.
6. Ponec, M., A. Weerheim, P. Lankhorst, and P. Wertz. 2003. New acylceramide in native and reconstructed epidermis. J. Invest. Dermatol. 120:581-588.
7. Robson, K. J., M. E. Stewart, S. Michelsen, N. D. Lazo, and D. T. Downing. 1994. 6-Hydroxy-4-sphingenine in human epidermal ceramides. J. Lipid. Res. 35:2060-2068.
8. Stewart, M. E., and D. T. Downing. 1999. A new 6-hydroxy-4-sphingenine-containing ceramide in human skin. J. Lipid. Res. 40:1434-1439.
9. Wertz, P. W., M. C. Miethke, S. A. Long, J. S. Strauss, and D. T. Downing. 1985. The composition of the ceramides from human stratum corneum and from comedones. J. Invest. Dermatol. 84:410-412.
10. Bouwstra, J. A., G. S. Gooris, W. Bras, and D. T. Downing. 1995. Lipid organization in pig stratum corneum. J. Lipid Res. 36:685-695.
11. Bouwstra, J. A., G. S. Gooris, J. A. van der Spek, and W. Bras. 1991. Structural investigations of human stratum corneum by small-angle X-ray scattering. J. Invest. Dermatol. 97:1005-1012.
12. Bouwstra, J. A., G. S. Gooris, F. E. Dubbelaar, and M. Ponec. 2001. Phase behavior of lipid mixtures based on human ceramides: coexistence of crystalline and liquid phases. J Lipid Res 42:1759-1770.
13. Bouwstra, J. A., G. S. Gooris, F. E. Dubbelaar, and M. Ponec. 2002. Phase behavior of stratum corneum lipid mixtures based on human

ceramides: the role of natural and synthetic ceramide 1. J Invest Dermatol 118:606-617.
14. Bouwstra, J., G. Gooris, and M. Ponec. 2002. The lipid organisation of the skin barrier: liquid and crystalline domains coexist in lamellar phases. journal of Biological Physics 28:211-223.
15. Hatta, I., N. Ohta, K. Inoue, and N. Yagi. 2006. Coexistence of two domains in intercellular lipid matrix of stratum corneum. Biochim Biophys Acta 1758:1830-1836.
16. White, S. H., D. Mirejovsky, and G. I. King. 1988. Structure of lamellar lipid domains and corneocyte envelopes of murine stratum corneum. An X-ray diffraction study. Biochemistry 27:3725-3732.
17. Wertz, P. 1991. Epidermal lipids. In Physiology, Biochemistry and Molecular Biology of the Skin. L. A. Goldsmith, editor. Oxford University Press, Oxford. 205-235.
18. Williams, M. L., and P. M. Elias. 1981. Stratum corneum lipids in disorders of cornification: increased cholesterol sulfate content of stratum corneum in recessive x-linked ichthyosis. J Clin Invest 68:1404-1410.
19. Elias, P. M., M. L. Williams, M. E. Maloney, J. A. Bonifas, B. E. Brown, S. Grayson, and E. H. Epstein, Jr. 1984. Stratum corneum lipids in disorders of cornification. Steroid sulfatase and cholesterol sulfate in normal desquamation and the pathogenesis of recessive X-linked ichthyosis. J Clin Invest 74:1414-1421.
20. Motta, S., S. Sesana, R. Ghidoni, and M. Monti. 1995. Content of the different lipid classes in psoriatic scale. Arch Dermatol Res 287:691-694.
21. Rogers, J., C. Harding, A. Mayo, J. Banks, and A. Rawlings. 1996. Stratum corneum lipids: the effect of ageing and the seasons. Arch Dermatol Res 288:765-770.
22. Zettersten, E., M. Q. Man, J. Sato, M. Denda, A. Farrell, R. Ghadially, M. L. Williams, K. R. Feingold, and P. M. Elias. 1998. Recessive x-linked ichthyosis: role of cholesterol-sulfate accumulation in the barrier abnormality. J Invest Dermatol 111:784-790.
23. McIntosh, T. J. 2003. Organization of skin stratum corneum extracellular lamellae: diffraction evidence for asymmetric distribution of cholesterol. Biophys J 85:1675-1681.
24. Kuempel, D., D. C. Swartzendruber, C. A. Squier, and P. W. Wertz. 1998. In vitro reconstitution of stratum corneum lipid lamellae. Biochim. Biophys. Acta 1372:135-140.
25. Bouwstra, J. A., G. S. Gooris, K. Cheng, A. Weerheim, W. Bras, and M. Ponec. 1996. Phase behavior of isolated skin lipids. J. Lipid Res. 37:999-1011.
26. de Jager, M., W. Groenink, R. Bielsa i Guivernau, E. Andersson, N. Angelova, M. Ponec, and J. Bouwstra. 2006. A novel in vitro percutaneous penetration model: evaluation of barrier properties

with p-aminobenzoic acid and two of its derivatives. Pharm. Res. 23:951-960.
27. de Jager, M., W. Groenink, J. van der Spek, C. Janmaat, G. Gooris, M. Ponec, and J. Bouwstra. 2006. Preparation and characterization of a stratum corneum substitute for in vitro percutaneous penetration studies. Biochim. Biophys. Acta 1758:636-644.
28. Gooris, G. S., and J. A. Bouwstra. 2007. Infrared spectroscopic study of stratum corneum model membranes prepared from human ceramides, cholesterol, and fatty acids. Biophys J 92:2785-2795.
29. Snyder, R. G., S. L. Hsu, and S. Krimm. 1978. Vibrational-Spectra in C-H Stretching Region and Structure of Polymethylene Chain. Spectrochimica Acta Part a-Molecular and Biomolecular Spectroscopy 34:395-406.
30. Wolfangel, P., R. Lehnert, H. H. Meyer, and K. Muller. 1999. FTIR studies of phospholipid membranes containing monoacetylenic acyl chains. Physical Chemistry Chemical Physics 1:4833-4841.
31. Snyder, R. G. 1960. Vibrational Spectra of Crystalline N-Paraffins .1. Methylene Rocking and Wagging Modes. Journal of Molecular Spectroscopy 4:411-434.
32. Moore, D. J., M. E. Rerek, and R. Mendelsohn. 1997. Lipid domains and orthorhombic phases in model stratum corneum: Evidence from Fourier transform infrared spectroscopy studies. Biochemical and Biophysical Research Communications 231:797-801.
33. Conti, A., J. Rogers, P. Verdejo, C. R. Harding, and A. V. Rawlings. 1996. Seasonal influences on stratum corneum ceramide 1 fatty acids and the influence of topical essential fatty acids. Int J Cosmet Sci 18:1-12.
34. Rerek, M. E., H. Chen, B. Markovic, D. van Wyck, P. Garidel, R. Mendelsohn, and D. J. Moore. 2001. Phytosphyngosine and Sphingosine Ceramide Headgroup Hydrogen Bonding: Structural Insights through Thermotropic Hydrogen/Deuterium Exchange. J Phys Chem B 105:9355-9362.
35. Janssens, M., G. S. Gooris, and J. A. Bouwstra. 2009. Infrared spectroscopy studies of mixtures prepared with synthetic ceramides varying in head group architecture: coexistence of liquid and crystalline phases. Biochim Biophys Acta 1788:732-742.
36. Garson, J. C., J. Doucet, J. L. Leveque, and G. Tsoucaris. 1991. Oriented structure in human stratum corneum revealed by X-ray diffraction. J Invest Dermatol 96:43-49.
37. Gomez-Fernandez, J. C., and J. Villalain. 1998. The use of FT-IR for quantitative studies of the apparent pKa of lipid carboxyl groups and the dehydration degree of the phosphate group of phospholipids. Chem Phys Lipids 96:41-52.
38. Rawlings, A. V., J. Hope, J. Rogers, A. M. Mayo, and I. R. Scott. 1992. Mechanisms of desquamation: new insights into dry flaky skin

conditions. In Proceedings of the 17th IFSCC International Congress. 865-880.

39. Rawlings, A. V., A. Watkinson, J. Rogers, A. M. Mayo, J. Hope, and I. R. Scott. 1994. Abnormalities in Stratum-Corneum Structure, Lipid-Composition, and Desmosome Degradation in Soap-Induced Winter Xerosis. Journal of the Society of Cosmetic Chemists 45:203-220.
40. Marks, J., S. Rogers, B. Chadkirk, and S. Shuster. 1981. Clearance of Chronic Plaque Psoriasis by Anthralin - Subjective and Objective Assessment and Comparison with Photochemotherapy. British Journal of Dermatology 105:96-99.
41. Bouwstra, J. A., G. S. Gooris, F. E. Dubbelaar, and M. Ponec. 1999. Cholesterol sulfate and calcium affect stratum corneum lipid organization over a wide temperature range. J Lipid Res 40:2303-2312.
42. Bouwstra, J. A., G. S. Gooris, F. E. Dubbelaar, A. M. Weerheim, and M. Ponec. 1998. pH, cholesterol sulfate, and fatty acids affect the stratum corneum lipid organization. J Investig Dermatol Symp Proc 3:69-74.